Journal of Molecular Structure 994 (2011) 269–275

Contents lists available at ScienceDirect

Journal of Molecular Structure

journal homepage: www.elsevier.com/locate/molstruc

Hydrogen bonding chains and rings structural motifs in new series of *N*-phthaloyl aminocarboxylic acid derivatives. Solid state microwave synthesis, structural chemistry, computational calculations and antimicrobial activity

Khalid Al-Farhan [a], Mohamed Ghazzali [a,*], Hassan M.A. Al-Hazimi [a], Ayman El-Faham [a,b], Jan Reedijk [a,c]

[a] Department of Chemistry, College of Science, King Saud University, P.O. Box 2455, Riyadh 11451, Saudi Arabia
[b] Chemistry Department, Faculty of science, Alexandria University, P.O. Box 426 Ibrahimia, 12321 Alexandria, Egypt
[c] Leiden Institute of Chemistry, Leiden University, P.O. Box 9502, 2300 RA, Leiden, The Netherlands

ARTICLE INFO

Article history:
Received 14 December 2010
Received in revised form 9 March 2011
Accepted 9 March 2011
Available online 25 March 2011

Keywords:
N-protected amino acid
Solid-state microwave synthesis
Hydrogen bonding
MP2/DFT calculations
Hirshfeld surfaces
Antimicrobial activity

ABSTRACT

A series of six *N*-phthaloyl aminocarboxylic acids were synthesized by using improved microwave irradiation with a multimode reactor. X-ray single crystal diffraction established the molecular structure of three *N*-protected aminocarboxylic acids derivatives, and spectral data agree with these in solution. The hydrogen bonding characteristics of this class of molecules are discussed on the basis of crystal structural analyses, *MP2/DFT* quantum calculations and Hirshfeld surfaces analyses. The relative strengths of the structural O–H···O and C–H···O hydrogen bonding chain and ring motifs are compared. Antimicrobial activities of 2-(1,3-dioxoisoindolin-2-yl)propanoic acid, 2-(1,3-dioxoisoindolin-2-yl)-3-phenylpropanoic acid and 2-(4-(1,3-dioxoisoindolin-2-yl)phenyl)acetic acid, were screened against three pathogenic strains; only the first two compounds were found to be quite sensitive against Gram +ve and Gram −ve bacterial strains, respectively. A relative structure–function relationship is observed.

1. Introduction

Phthalimide derivatives are widely used as anesthetics [1], DNA cleaving agents [2,3], tumoricidals and optical brighteners [4,5], as well as dyes [6]. They are known also as fluoroprobes [7] with interesting photophysical properties [8,9]. Pyromellitic di-anhydride is an analogous compound, which undergoes facile polymerization reaction with diamines to give amide or imides containing polymers. It also has a relevance to nanomaterials [10], as compounds analogous to phthalimides are self-assembling to form nano-tube like structures [11–13]. Moreover, the *N*-phthaloyl derivatives showed many host–guest chemical applications [14–17], and recently were used as an organic ligand for new anticancer metal complexes [18].

The *N*-phthaloylglycine is a simple *N*-protected aminocarboxylic acid with interesting supramolecular features on formation of metal coordination complexes [19]. Because of the great importance of amino acids in physiological and pharmacological events [20–22], and due to the role of *N*-protected aminocarboxylic acids in peptide synthesis, it appeared worthwhile to search for a simple, clean and convenient method for the preparation of such *N*-phthaloyl aminocarboxylic acid derivatives, which so far had been prepared only by conventional methods [23].

Solid-state microwave-assisted organic synthesis is recognized as one of the interesting areas of current chemical research and technology [24–26]. Coupling of microwave irradiation with the use of catalysts, under solvent-free conditions, provides a clean chemical process with enhanced reaction rate, higher yield and purity [27–29]. In a very recent report, we showed the syntheses of *N*-phthaloyl aminocarboxylic acid derivatives using a domestic microwave with a solvent-free method [30]. The present work describes the syntheses of *N*-phthaloyl aminocarboxylic acids by employing a microwave multimode reactor (Synthos 3000 Aton Paar, GmbH, 1400 W maximum magnetron) with excellent yields and high product purity.

To structurally characterize the compounds, X-ray single crystal structure determinations for three of the new *N*-phthaloyl aminocarboxylic acids derivatives were performed and the roles of hydrogen bonding O–H···O and C–H···O motifs in the three structures were investigated in the light of *MP2/DFT* quantum chemical calculations and Hirshfeld surfaces analyses. Finally, the antimicrobial activities for a selection of three derivatives (**2**, **5**, and **7** in Scheme 1) were tested against *Staphylococcus aureus* ATCC6538, *Escherichia coli* ATCC25292 and *Candida albican* strains; only compounds **2** and **5** were found to be sensitive against Gram +ve and

* Corresponding author. Tel.: +966 1 4675970; fax: +966 1 4675992.
E-mail address: mghazzali@ksu.edu.sa (M. Ghazzali).

0022-2860/$ - see front matter © 2011 Elsevier B.V. All rights reserved.
doi:10.1016/j.molstruc.2011.03.030

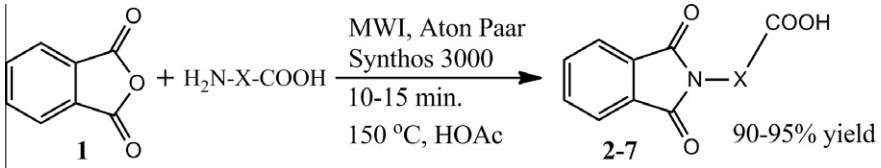

X = $CH(CH_3)$; **2**
X = $CH(CH(CH_3)_2$(L); **3**
X = $CH(CH(CH_3)_2$(DL); **4**
X = $CH(CH_2$-$C_6H_5)$; **5**
X = C_6H_4; **6**
X = C_6H_4-CH_2-; **7**

Scheme 1. Microwave syntheses of 6 new *N*-Phthaloyl aminocarboxylic acids.

Gram −ve bacterial strains, respectively, with no sensitivity for *E. Coli* was detected.

2. Experimental

2.1. Syntheses and characterization

^1H and ^{13}C NMR spectra were recorded on a JEOL ECP 400 NMR spectrometer operating at 400 MHz in $CDCl_3$ unless otherwise specified with TMS as internal standard. Chemical shifts are given in ppm and coupling constants (*J*) are given in Hz. The full solution characterizations, as based on ^1H and ^{13}C NMR spectral data are given below. Melting points have been determined on an electrothermal's IA9000 series digital capillary melting point apparatus and are uncorrected. Microwave irradiations (abbreviated MWI) were performed by employing a multimode reactor (Synthos 3000 Aton Paar, GmbH, 1400 W maximum magnetron).

2.1.1. N-phthaloyl-L-alanine (**2**)

White crystals, m.p. 106 °C; ^1H NMR($CDCl_3$): ppm 1.67(d, *J* = 7.32 Hz, 3H), 4.99(d, *J* = 7.32 Hz, 1H), 7.67–7.71(dd, 2H), 7.79–7.82(dd, 2H), 10.67(s, OH); ^{13}C NMR: δ 15.07(CH_3), 47.32(CH), 123.67(d, 2C), 131.78(s,2C), 134.36(d,2C), 167.50(2C=O), 175.61(C=O).

2.1.2. N-phthaloyl-L-alanine (**3**)

White crystals, m.p. 78 °C; ^1H NMR($CDCl_3$): ppm ^1H NMR: ppm 0.86 and 1.13(each d, *J* = 7.3 Hz, 2 × 3H), 2.04(m, 1H), 4.57(d, *J* = 7.4 Hz, 1H), 7.68–7.77(dd, 2H), 7.81–7.83(dd, 2H), 12.82(s, OH); ^{13}C NMR: ppm 19.53 and 19.57(2 × CH_3), 28.42(CH), 57.94(CH), 123.66(d, 2C), 131.59(s,2C), 134.48(d,2C), 167.91(2C=O), 174.09(C=O).

2.1.3. N-(DL)Phthaloylvaline (**4**)

White crystals, m.p. 84 °C; ^1H NMR($CDCl_3$): ppm ^1H NMR: ppm 0.81 and 0.82(each d, 2 × 3H (D-isomer), 1.05 and 1.07(each d, 2 × 3H (L-isomer), 2.51–2.58(m, 1H), 4.45(d, *J* = 8.0 Hz, 1H), 7.88–7.91(m, 4H), 13.07(brs, OH); ^{13}C NMR: ppm 19.73 and 21.3(2 × CH_3), 28.42(CH), 57.42(CH), 123.95(d,2C), 131.46(s,2C), 135.41(d,2C), 167.99(2C=O), 170.39(C=O).

2.1.4. N-phthaloyl-L-alanine (**5**)

White prisms, m.p. 156–157 °C; ^1H NMR: ppm 3.58(d, *J* = 8.8 Hz, 2H), 5.22(t, *J* = 8.8 Hz, 1H), 7.66(m, 2H), 7.76(m, 2H), 9.94(s, OH); ^{13}C NMR: ppm 34.35, 53.17, 123.66(d, 2C), 127.04, 128.7(d,2C), 128.9(d,2C), 131.51(s,2C), 134.29(d,2C), 167.53(2C=O), 174.75(C=O).

2.1.5. 4-(N-Phthaloyl)aminobenzoic acid (**6**)

White plates, m.p. 270–272 °C; ^1H NMR: ppm 7.61(d, *J* = 8.8 Hz, 2H), 7.90–7.94(m, 2H), 7.97–8.01(m, 2H), 8.04(d, *J* = 8.8 Hz, 2H), 13.3(s, OH); ^{13}C NMR: 124.11(d,2C), 127.56(d,2C), 130.39(d,2C), 130.55(s), 132.05(s,2C), 135.39(d,2C), 136.38(s), 167.29(2C=O), 167.21(C=O).

2.1.6. 4-(N-Phthaloyl)phenyl)acetic acid (**7**)

White prisms, m.p. 180–181 °C; ^1H NMR: ppm 3.89(s,CH_2), 7.40–7.49(m, 4H), 7.77–7.80(m, 2H), 7.94–7.96(m, 2H), 9.68(s,OH); ^{13}C NMR: 123.86(d,2C), 126.73(d,2C), 130.21(d,2C), 130.55(s), 131.81(s,2C), 134.50(d,2C), 136.38(s), 168.50(2C=O), 168.1(C=O).

3. Crystal structure determinations

Suitable single crystals of compounds **2, 5** and **7** were selected under an optical microscope, glued and mounted onto thin glass capillary. Diffraction data were collected using a Rigaku *R*-axis SPIDER diffractometer equipped with imaging plate area detector utilizing Mo Kα radiation (λ = 0.71073 Å) with graphite monochromator. The data were collected using ω-scans at a temperature of 294 ± 2 K to a maximum 2θ of 55.0°. Preliminary orientation matrices, unit cell determination, data reduction and absorption correction were performed using Crystal Clear package [31]. The data were corrected for Lorentz and polarization effects.

Structures were solved by direct methods and refined by full-matrix least squares on all $|F^2|$ data using SHELX packages [32]. Hydrogen atoms were isotropically refined and constrained to ideal geometry, using their appropriate riding model and non-hydrogen atoms were anisotropically refined. The crystallographic descriptive figures were created using the DIAMOND package [33]. Graph-Set analyses and hydrogen bonding network assignments were performed with the aid of RPluto [34].

4. Theoretical calculations

Single-point quantum calculations for **2**, **5** and **7** were made with the *ab initio* DFT module in Spartan 08-version 1.2.0 [35], using the exchange and correlation functional of Becke and Perdew (BP86) [36,37] as a perturbation on self consistent density with the 6-31G* basis set. This Generalized Gradient Approximation (GGA) functional with 6-31G* basis set which includes polarization functions on non-hydrogen atoms [38], is known to show reliable results with organic molecules and is usually a good compromise between accuracy and computational demands [39,40]. The electrostatic density potential was calculated with the restricted correlation functional *MP2* post-Hartree–Fock level of theory.

Traditionally, MP2 has been known to consistently provide a precise description of hydrogen bonding [41,42]. These calculations have been carried out with a high accuracy large integration grid, so that sensitivity is minimized. The starting *z*-matrix was imported from the single crystal structure coordinates and used without geometrical constraints. Hirshfeld surfaces [43] were analyzed with the CrystalExplorer 2.1 package [44].

5. Antimicrobial activity

The disc diffusion method was employed for the determination of antibacterial activity using agar nutrient as the medium [45]. *S. aureus* ATCC6538, *E. coli* ATCC25292 and *C. albican* (clinic isolate) strains were used as bacterial pathogens. 50% w/v Stock solutions were prepared by dissolving the compounds in EtOH. In a typical procedure, a well was made on the agar medium inoculated with microorganisms. The well was filled with the test solution using a micropipette and the plate was incubated at 310 K for 24 h after being kept at refrigerator for 2 h. During this period, the test solution is diffused and the growth of the inoculated microorganism is examined. Controls were also examined using only EtOH. The diameters of the inhibition zones were measured in millimeters.

6. Results and discussion

With the wide applications of microwave-mediated synthesis of organic compounds, only little work has appeared about *N*-phthaloyl aminocarboxylic acids. In 1995 Bose et al. [46] reported that *N*-phthaloyl aminocarboxylic acids could be synthesized within a few minutes in good yields using microwave irradiation in DMF. Also, Vidal et al. reported [47] the use of the same technique for the synthesis of phthalimides. Among them, *N*-phthaloylglycine was obtained in 90% and 95% yields in xylene and DMF, respectively. However, at the end of irradiation of these syntheses, the products usually extracted with acetone. Here we apply a solvent-free methodology by using the microwave irradiation and compare it against the conventional method. The detailed synthetic procedures used for conventional and microwave methods and the two respective yields are given in the Supplementary material. The supplemented results are illustrating the significantly higher yields with MWI.

Each aminocarboxylic acid was mixed with phthalic anhydride (**1**) in acetic acid inside a reaction vessel and placed in the corresponding rotor, fixed by screwing down the upper rotor place, and finally the rotor was closed with a protective hood [48]. After heating the vessels for 10 min. at 150° (~10 bar, 1000 W), cooling was accomplished by a fan (5 min), and the workup for the vessel was performed as described in the Supplementary material.

The used microwave method proved also to be safe in terms of racemization. This was confirmed by the synthesis of authentic sample from *N*-phthaloyl-(L)-valine and *N*-phthaloyl-(DL)-valine. The ^{1}H NMR did not detect any of the D-valine in the pure sample of the L-isomer (L-isomer at 1.05 and 1.07 ppm and D-isomer at 0.81 and 0.82 ppm).

Crystals suitable for diffraction experiments were collected directly from the microwave vessels and used without further treatments. The conventional synthesis failed to produce single crystals without recrystallization attempts. The crystallographic data are summarized in Table 1, while selected bond distances and bond angles are given in Table 2. The thermal crystal structure ellipsoidal drawings for **2**, **5** and **7** with their atomic numbering schemes are depicted in Fig. 1. The crystal structures of 2-(1,3-dioxoisoindolin-2-yl)propanoic acid **2**, 2-(1,3-dioxoisoindolin-2-yl)-3-phenylpropanoic acid **5**, and 2-(4-(1,3-dioxoisoindolin-2-yl)phenyl)acetic acid **7** are all crystallized in the monoclinic crystal system with interatomic bond distances and angles are within normal ranges; see Table 2.

Table 1
Crystal data and refinement details for compounds **2**, **5** and **7**.

	2	**5**	**7**
Formula	$C_{11}H_9N_1O_4$	$C_{17}H_{13}NO_4$	$C_{16}H_{11}NO_4$
Formula weight	219.19	295.28	281.26
Crystal system	Monoclinic	Monoclinic	Monoclinic
Space group	$P2_1/c$	$P2_1$	$P2_1/a$
a (Å)	9.879(2)	9.5206(4)	7.1548(2)
b (Å)	10.704(2)	5.8295(3)	16.6282(6)
c (Å)	10.090(2)	13.0050(7)	11.3487(4)
alpha (°)	90	90	90
beta (°)	93.27(3)	92.6640 (10)	90.921(1)
gamma (°)	90	90	90
V (Å^3)	1065.2(4)	721	1350.00(8)
Z	4	2	4
D (calc) (g/cm^3)	1.367	1.36	1.384
Theta min–max (°)	3.4, 27.5	3.1, 27.5	3.0, 27.5
Tot., uniq. data, *R*(int)	12251, 2434, 0.048	9801, 1817, 0.031	29450, 3102, 0.033
Observed data [*I* > 2.0 sigma(*I*)]	1438	1395	2218
*N*ref, *N*par	2434, 147	1817, 201	3102, 191
R, wR_2, *S*	0.0505 0.1688, 1.01	0.039, 0.131, 1.01	0.0404, 0.1353, 1.00
Max. and av. shift/error	0.00, 0.00	0.00, 0.00	0.00, 0.00
Min. and max. resd. dens.	−0.19, 0.16	0.18, 0.16	−0.20, 0.12
Flack parameter		0(10)	

Table 2
Selected bond distances (Å) and angles (°) for compounds **2**, **5** and **7**.

2		O(3)–C(10)	1.321(3) Å
O(1)–C(7)	1.206(3) Å	O(4)–C(10)	1.191(4) Å
N(1)–C(7)	1.395(3) Å	N(1)–C(9)	1.447(3) Å
C(1)–C(6)	1.374(3) Å	C(10)–O(3)–H(3A)	110°
O(2)–C(8)	1.208(3) Å	C(7)–N(1)–C(8)	111.2(2)°
N(1)–C(8)	1.391(3) Å	C(7)–N(1)–C(9)	122.1(2)°
O(3)–C(10)	1.273(3) Å	C(8)–N(1)–C(9)	126.0(2)°
N(1)–C(9)	1.459(3) Å	**7**	
O(4)–C(10)	1.240(2) Å	O(1)–C(7)	1.208(2) Å
C(10)–O(3)–H(3A)	110°	O(2)–C(8)	1.211(2) Å
C(7)–N(1)–C(8)	112.0(2)°	O(3)–C(10)	1.317(2) Å
C(7)–N(1)–C(9)	124.2(2)°	O(4)–C(10)	1.213(1) Å
C(8)–N(1)–C(9)	123.2(2)°	N(1)–C(9)	1.432(2) Å
5		N(1)–C(7)	1.411(2) Å
O(1)–C(7)	1.206(4) Å	C(10)–O(3)–H(3A)	109°
O(2)–C(8)	1.219(3) Å	C(7)–N(1)–C(8)	111.1(1)°
N(1)–C(7)	1.412(3) Å	C(7)–N(1)–C(9)	124.7(1)°
N(1)–C(8)	1.382(4) Å	O(1)–C(7)–N(1)	124.9(1)°

While one carbon atom (C9) is defined to have a chiral configuration in both **2** and **5**, only the 2-(1,3-dioxoisoindolin-2-yl)-3-phenylpropanoic acid **5** is crystallized in the Sohncke space group $P2_1$. The absolute structure cannot be unambiguously determined from the present refinement. However, the Flack parameter [49] of 0.0(10) suggests that the chosen polarity is correct.

In the crystal structures of **2, 5** and **7** the overall conformation of the isoindoline-1,3-dione is planar with the maximum deviations from the least-square best fit plane for the nine atoms in **2** being −0.0388 (3) Å for atom N1 below the plane and atom C8 with 0.0332 (1) Å above the plane. The maximum deviations in **5** and **7** are found to be −0.0331 (2) Å for atom C8, 0.0275 (4) Å for atom N1 and −0.0260 (2) Å for atom C8, 0.0371 (1) Å for atom C3 in **5** and **7**, respectively. In **2**, the dihedral angle between the least-squares plane to the nine atoms of the isoindoline-1,3-dione (C1 to C8 and N1) and the least-squares plane of the carboxylic group (C10, O3, O4 and H3A) is 83.898(7)°.

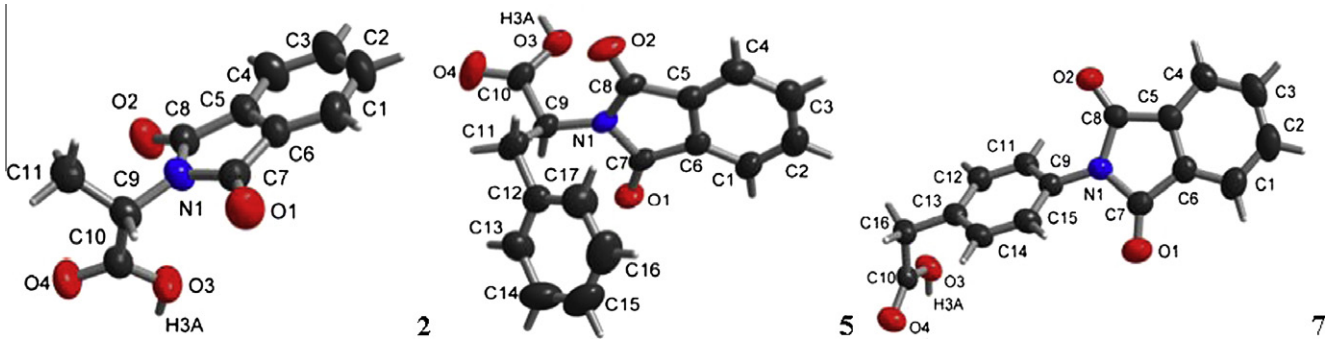

Fig. 1. Atomic numbering scheme of **2**, **5**, and **7** with atomic displacement ellipsoids shown at 50% probability level.

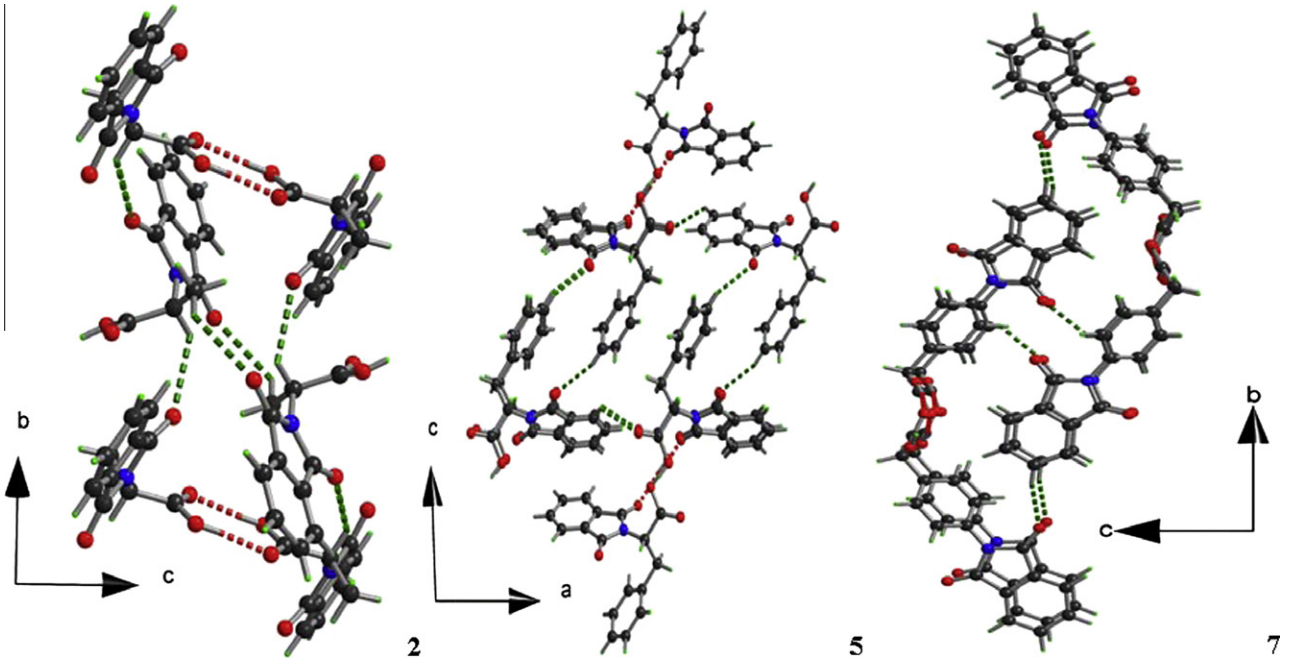

Fig. 2. Perspective drawing of the structures in **2**, **5** and **7** showing the intermolecular O–H···O and C–H···O hydrogen bonding. The O–H···O and C–H···O hydrogen bonding are represented as red and green dashed lines, respectively. For symmetry codes, see Table 3. (For interpretation of the references to colour in this figure legend, the reader is referred to the web version of this article.)

A view of the crystal packing in **2**, **5** and **7** is depicted in Fig. 2. The primary hydrogen-bond interaction is the formation of an $R_2^2(8)$ O–H···O second-level ring motif [50] dimers from two identical carboxylic groups. These strong O–H···O dimers are augmented in the *bc*-plane with C(5) first-level chain (C9–H9···O2) in the *b*-direction and $R_2^2(12)$ (C11–H11B···O1) ring motifs C–H···O non-classical hydrogen bonding. Both C–H···O motifs could be regarded as a $C_2^2(11)$ second-level chain motif, featuring a two-dimensional bilayered network structure. In Table 3, all hydrogen bonding geometric details for **2**, **5** and **7** are presented, for both O–H···O and C–H···O interactions.

In **5**, the dihedral angle between the least-squares plane to the nine atoms of the isoindoline-1,3-dione (C1 to C8 and N1) and the least-squares plane of the carboxylic group (C10, O3, O4 and H3A) is 60.854(1)°. The dihedral angle between least-squares best-fit plane to the aromatic six atoms of the phenyl ring (C12 to C17) and the least-squares plane to the carboxylic group is 51.424(2)°. The molecular arrangement in **5** is governed with both O–H···O and weak C–H···O hydrogen bonding interactions. The O–H···O interactions are extending in between the carboxylate oxygen (O3) and one of the dione oxygen (O1) featuring C(6) first-level chain motif affording a crankshaft-like array in the *b*-direction. These arrays are supported with a C(10) first-level chain motif (C15–H15···O1) in the *c*-direction and a C(8) chain motif in the *a*-direction (C3–H3···O4). Both motifs can be regarded together as forming a $C_2^2(18)$ second-level chain motif extending in the *ac*-plane that furnishing a 3D-hydrogen bonding network. Moreover, the structure of **5** shows also a strong C–H···π interaction at H···π distance of 2.99 Å and C–H···π angle of 128° in-between the isoindoline-1,3-dione aromatic rings.

In **7**, the dihedral angle between the least-squares plane to the nine atoms of the isoindoline-1,3-dione (C1 to C8 and N1) and the least-squares plane of the carboxylic group (C10, O3, O4 and H3A) is 79.11(4)° and the angle between least-squares best-fit plane to the aromatic six atoms of the phenyl ring (C9 and C11 to C15) and the least-squares plane of the carboxylic group is 74.53(5)°. In comparison with **2** and **5**, a crankshaft-like array in the *a*-direction is formed by C(4) O–H···O hydrogen-bonding first-level chain motif, extending in between the carboxylate oxygen (O3 and O4) of **7**. These *a*-direction crankshafts are further augmented with C–H···O interactions in the *b*-direction (C3–H3···O1) with a C(7) chain motif, as well as $R_2^2(12)$ second-level ring motif (C15–H15···O1) in the *bc*-plane. A combination of the non-classical C–H···O hydrogen bonding motifs as

Table 3
Hydrogen bonding geometries for **2**, **5** and **7**.

D–H···A	*d*(H···A)	*d*(D···A)	∠(DHA)
2			
O3–H3A···O4^{i}	1.79	2.602(2)	170
C9–H9···O2^{ii}	2.7	3.292(2)	119
C11–H11B···O1^{iii}	2.71	3.452(3)	135
(i) 1 − *x*, 1 − *y*, −*z*. (ii) 1 − *x*, *y* − 0.5, 0.5 − *z*			
(iii) 1 − *x*, 1 − *y*, 1 − *z*			
5			
O3–H3A···O1^{i}	1.95	2.766(3)	171
C15–H15···O1^{ii}	2.56	3.440(3)	158
C3–H3···O4^{iii}	2.67	3.328(4)	128
(i) 1 − *x*, −1/2 + *y*, −*z*. (ii) 2 − *x*, 1/2 + *y*, 1 − *z*			
(iii) *x* − 1, *y* − 1, *z*			
7			
O3–H3A···O4^{i}	1.87	2.649(1)	159
C15–H15···O1^{ii}	2.59	3.319(2)	136
C3–H3···O1^{iii}	2.63	3.460(2)	148
(i) −1/2 + *x*, 3/2 − *y*, *z*. (ii) 1 − *x*, 1 − *y*, 1 − *z*			

forming $C_2^2(13)$ second-level chain motif with the primary C(4) conventional O–H···O chain interaction, generates a 3D-hydrogen bonding network.

The complementary role of weak hydrogen bonding for directing the packing pattern, even in presence of strong interactions, is well documented. [50–54] However, not every hydrogen bonding contact, regardless of geometry parameters, is considered to be a hydrogen bond if it has non-negative interaction energies [55–58]. What remains undisputed is that there are certain types of weak hydrogen bonds, when complying with energy restrictions, are indistinguishable from classical hydrogen bonds [52–62].

In order to validate the contribution effect of C–H···O interaction energies in guiding the packing preferences of **2**, **5** and **7** and further in the construction of hydrogen bonding network in the three phthalimide derivatives, we have investigated its role by using theoretical calculations.

Calculations of hydrogen bonding enthalpy energies are by definition quite vague, since in the molecular solid state, hydrogen bonds are naturally deviating from optimal geometry. Also, during the calculation, the effective non-additive networks of hydrogen-bond energies are split into individual hydrogen bond entities [54,63–65].

Instead, we have therefore calculated the molecular electronic density and electrostatic density potentials. Second-order Møller–Plesset perturbation theory (MP2) is an affordable *ab initio* post Hartree–Fock quantum calculation for closed-shell S- and P-orbitals of reasonable molecular size [66,67]. The restricted MP2 correlation-corrected density matrix converges at energy slightly higher than the Self Consistent Field (SCF) gradient with *ca.* 30.43, 39.21, and 31.23 eV cut-off in **2**, **5**, and **7**, respectively. In the three calculations, the hydroxyl group *s*- and *p*-characters showed the complete localization at HOMO-4 and -5 levels of energy. In **2**, the single point calculations revealed uneven distribution of the HOMO/LUMO over the isoindoline-1,3-dione and the HOMO shows a minute contribution from carboxylic group and the LUMO defines a major contribution comes from the dione oxygen atoms; this is consistent with its role as C–H hydrogen bonding acceptor atoms. In **5**, the HOMO is delocalized over the phenyl ring with and the LUMO is only restricted over the isoindoline-1,3-dione part, and that is the same for LUMO of **7** while HOMO delocalization is featuring a higher area volume than those of **2** or **5** by extending over the phenyl part, with minor contributions from the isoindoline-1,3-dione as well as the carboxylic group.

Fig. 3 depicts the isosurfaces of electronic density and electrostatic density potential. In **2**, **5** and **7**, the highest positive electronic density or the highest delocalization parameters is defined around the slightly acidic-nature hydrogen atom of the carboxylic group and is also pointing outwards the space volume of the electrostatic density potentials. However, the localized potential energy values for the carboxylic hydrogen are different in **2**, **5** and **7** and are changing from *ca.* 312 kJ/mol in **2** to *ca.* 254 kJ/mol in **5** and *ca.* 257 kJ/mol in **7**. Also, a gradual increase of the oxygen atoms potential energy contributions is observed when going from the dione oxygen atoms to the hydroxyl one, which shows in **2** the highest value; this is again consistent with the variation of O–H···O hydrogen bonding network assignments from ring carboxylic dimers in **2** to chain motifs in **5** and **7,** and further with both interaction geometries (Table 3). The electrostatic density potential is intensively localized at the carboxyl O–H···O hydrogen-bonding acceptor atoms and also is the highest in **2,** but also is extended into the space volume between the oxygen C–H···O hydrogen bonding acceptor atoms of the dione. There is a clear discrimination on the scale of electronic density between carboxyl and aromatic hydrogen atoms, although their effects on the electrostatic density potential of hydrogen bonding to dione oxygen acceptor atoms are unambiguous.

We have been motivated to quantitatively analyze the individual contributions of the aromatic and carboxylic hydrogen atoms within the structural packing preferences. In order to quantify and compare the effect of O–H···O interactions in guiding the molecular packing preferences of **2**, **5** and **7**, we aimed to study its procrystal electronic density. The Hirshfeld surfaces, based on the Hirshfeld stockholder partitioning scheme [43], fragmenting the electron densities as a crystal property [68–70] by employing the spherically averaged atomic densities derived from Clementi and Roetti's near Hartree–Fock atomic wave functions using the whole-of-molecule approach [71].

Fig. 4 depicts the d_{norm} Hirshfeld curvatures for **2**, **5** and **7** and is displayed using a blue–red–white color scheme, where red high-

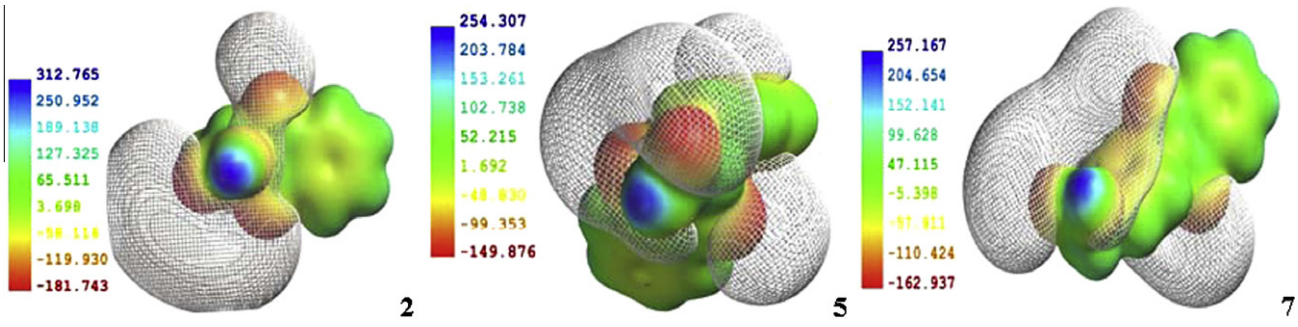

Fig. 3. Isosurfaces of electronic density (solid in green–blue) and isoelectrostatic potentials (mesh in gray) for **2**, **5** and **7** calculated by DFT and MP2. Mesh isosurfaces are in the range +5 eV to −5 eV. Scales for electronic density are given in kJ/mol. (For interpretation of the references to color in this figure legend, the reader is referred to the web version of this article.)

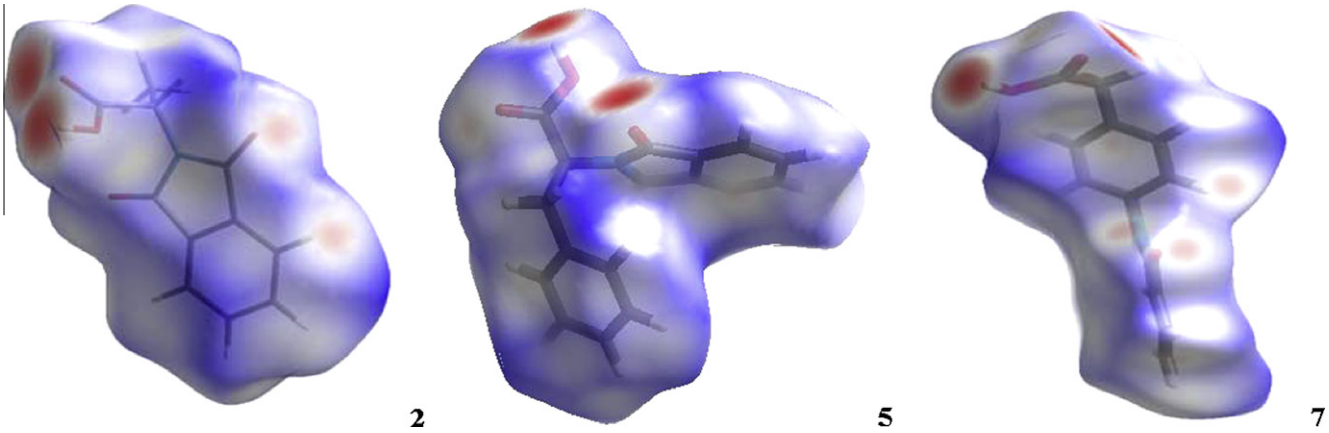

Fig. 4. Hirshfeld surface of **2**, **5** and **7** mapped with normalized electronic density.

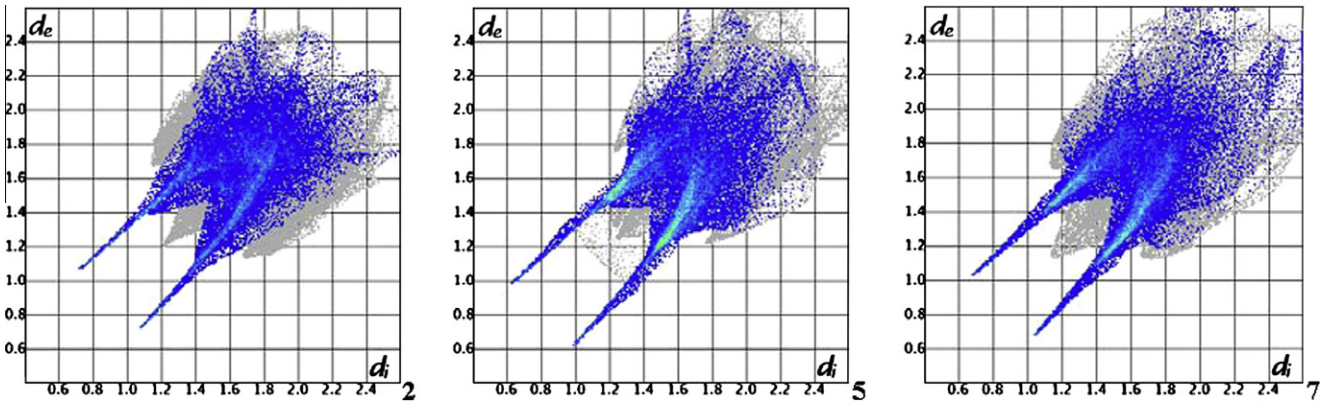

Fig. 5. 2D-fingerprint plots for **2**, **5** and **7** resolved into O–H···O contacts. The full fingerprint appears beneath in gray shadow.

lights shorter contacts, white for contacts around the vdW separation and blue for areas with no interaction contacts.

Two intense and large red spots, as the internuclear separations decrease, are observed at the carboxylate O atoms in **2**. Two faint and small spots are also visible at the dione O atom and aromatic H that specify the C–H···O contacts. In Fig. 5, two-dimensional fingerprint plots of the intermolecular interactions in the molecular crystal of **2**, **5** and **7** are presented; the values of d_e and d_i correspond to distances to the nearest atoms outside and inside the molecule, where hydrogen is the closest atom inside the surface, and oxygen is the nearest atom outside the surface, and *vice versa*.

The area of the highlighted surface for the O–H···O interaction in **2** comprises *ca.* 67% of the total Hirshfeld surface area for this molecule. In **5** and **7**, similar Hirshfeld surface partitioning scheme analyses were performed and O–H···O interactions were resolved into *ca.* 48% and 52% of the total Hirshfeld surface area in **5** and **7**, respectively.

Thus, although the classical O–H···O hydrogen bonding ring motif in **2** contributes to a larger amount than in **5** or **7**, still the non-conventional C–H···O shows an important addition to the total Hirshfeld surfaces. So from a detailed description of the hydrogen bonding structural features for **2**, **5**, and **7** on the basis of both O–H···O and C–H···O we have shown by theoretical calculations the complementary role of weak interactions in presence of strong ones.

The *in vitro* antipathogenic activity of a selection of compounds, *i.e.* **2**, **5** and **7,** has been screened against the *S. aureus* ATCC6538, *E. coli* ATCC25292 and *C. albican* (clinic isolate) strains. The results show a variable activity. Compound **2** displays a quite high sensitivity against *S. aureus* with an inhibition zone of 17 mm, while compound **5** showed a good sensitivity against *C. albican* with an inhibition zone of 19 mm. Both compounds **2** and **5** were found to be less effective than the use reference substances (chloramphenicol yielding a 22 mm inhibition zone for *S. aureus* and Ketoconazol and with a 27 mm inhibition zone for *C. albicans*). *E. coli* was found to be resistant against **2**, **5** and **7**. Compound **7** shows no significant activity for all used lines. In summary, only compounds **2** and **5** were found to be sensitive against Gram + *ve* and Gram – *ve* bacterial strains. The higher activity of **2** and **5** can be attributed to the existence of acetyl group directly attached to the dione moiety, a structural character that is discontinued with **7**. Further studies on related compounds, as well as on the antimicrobial and antibacterial activity of the prepared phthalimide series are under investigation in our laboratory.

7. Concluding remarks

The result discussed above present the improved synthesis of new phthalimide derivatives, by employing microwave irradiation as a safe, fast and easy-to-use technique for the preparation of *N*-phthaloyl aminocarboxylic acids. Microwave irradiation (MWI) leads to many advantages, like the use of inexpensive reagents, in addition to the eco-friendly "green chemistry" environmental impacts. We have presented the relative contributions of hydrogen bonding in ring and chain motifs and shown that their interaction energies are further contributes and guides the molecular packing. A guide for the antimicrobial structure–function relationship for

these phthalimide derivatives was noticed to be related to the presence of a dione–acetyl group conjugation.

Acknowledgements

The authors are indebted to the Scientific Research Center, College of Science (Project No. Chem-2010/11) and to the Distinguished Scientist Fellowship Program (DSFP) at King Saud University, Riyadh, Saudi Arabia for supporting this work.

Appendix A. Supplementary material

Contained in the supplementary data are a more detailed presentation of microwave and conventional synthetic procedures and its yields comparison. CCDC 778829–778831 contains the supplementary crystallographic data for this paper. These data can be obtained free of charge via www.ccdc.cam.ac.uk/conts/retrieving.html or from Cambridge Crystallographic Data Centre (CCDC), 12 Union Road, Cambridge CB2 1EZ, UK; fax: +44 (0)1223 336033. Supplementary data associated with this article can be found, in the online version, at doi:10.1016/j.molstruc.2011.03.030.

References

[1] A. Dasettimo, G. Primofiore, P.L. Ferrarini, M. Ferretti, P.L. Barili, N. Tellini, P. Bianchini, Eur. J. Med. Chem. 24 (1989) 263.
[2] M.F. Brana, M. Cacho, A. Ramos, M.T. Dominguez, J.M. Pozuelo, C. Abradelo, M.F. Rey-Stolle, M. Yuste, C. Carrasco, C. Bailly, Org. Biomol. Chem. 1 (2003) 648.
[3] M.F. Brana, A. Ramos, Curr. Med. Chem. 1 (2001) 237.
[4] C.W. Schellhammer, J. Schroeder, Angew. Chem. Int. Ed. 14 (1975) 665.
[5] W.W. Stewart, Nature 292 (1981) 17.
[6] B. Ramachandram, A. Samanta, Chem. Commun. (1997) 1037.
[7] T.C. Barros, S. Brochsztain, V.G. Toscano, P. Berci, M.J. Politi, J. Photochem. Photobiol. A – Chem. 111 (1997) 97.
[8] M.J. Ahrens, L.E. Sinks, B. Rybtchinski, W.H. Liu, B.A. Jones, J.M. Giaimo, A.V. Gusev, A.J. Goshe, D.M. Tiede, M.R. Wasielewski, J. Am. Chem. Soc. 126 (2004) 8284.
[9] P. Yan, A. Chowdhury, M.W. Holman, D.M. Adams, J. Phys. Chem. B109 (2005) 724.
[10] M.W. Holman, R.C. Liu, D.M. Adams, J. Am. Chem. Soc. 125 (2003) 12649.
[11] N. Barooah, R.J. Sarma, J.B. Baruah, Cryst. Growth Des. 3 (2003) 639.
[12] N. Kimizuka, T. Kawasaki, K. Hirata, T. Kunitake, J. Am. Chem. Soc. 117 (1995) 6360.
[13] K. Kishikawa, S. Tsubokura, S. Kohmoto, M. Yamamoto, K. Yamaguchi, J. Org. Chem. 64 (1999) 7568.
[14] J.E.D. Davies, P. Finocchiaro, F.H. Herbstien, J.L. Atwood, J.E.D. Davies, D.D. MacNicol, Inclusion Compounds, vol. 2, Academic press, New York, 1984.
[15] A.A. Elasmy, M.A. Hafez, E.M. Saad, F.I. Taha, Trans. Met. Chem. 19 (1994) 603.
[16] F. Jaber, F. Charbonnier, R. Faure, Acta Cryst. C 51 (1995) 1765.
[17] G.K. Sandhu, S.S. Sandhu, Synth. React. Inorganic Met. – Org. Chem. 25 (1995) 93.
[18] S. Gomez-Ruiz, B. Gallego, M.R. Kaluderovic, H. Kommera, E. Hey-Hawkins, R. Paschke, G.N. Kaluderovic, J. Organomet. Chem. 694 (2009) 2191.
[19] L.H. Abdel-Rahman, Trans. Met. Chem. 26 (2001) 412.
[20] E. Eliel, S.H. Willen, L.N. Mander, Stereochemistry of Organic Compounds, Wiley, New York, 1994.
[21] E. Juaristi, Introduction to Stereochemistry and Conformational Analysis, Wiley, New York, 1991.
[22] E. Juaristi, An. Quim. 93 (1997) 135.
[23] A.H. Bedair, F.M. Ali, A.M. El-Agrody, F.A. Eid, M.A.A. El-Nassag, G. El-Sherbeny, Acta Pharm. 56 (2006) 273.
[24] S. Caddick, Tetrahedron 51 (1995) 10403.
[25] P. Lidstrom, J. Tierney, B. Wathey, J. Westman, Tetrahedron 57 (2001) 9225.
[26] L. Perreux, A. Loupy, Tetrahedron 57 (2001) 9199.
[27] A. Loupy, C. R. Chim. 7 (2004) 103.
[28] R.S. Varma, Tetrahedron 58 (2002) 1235.
[29] R.S. Varma, R. Dahiya, S. Kumar, Tetrahedron Lett. 38 (1997) 2039.
[30] H.M.A. Al-Hazimi, A. El-Faham, M. Ghazzali, K. Al-Farhan, Arab. J. Chem. (2010), doi:10.1016/j.arabjc.2010.06.020.
[31] Rigaku, Crystal Clear, Crystal Structure Analysis Package, Rigaku, 9009 New Trails Dr., The Woodlands, TX 77381, 2007.
[32] G.M. Sheldrick, Acta. Cryst. A 64 (2008) 112.
[33] Diamond, Crystal Impact GbR ver 3.1e (2007) Bonn, Germany.
[34] W.D.S. Motherwell, G.P. Shields, F.H. Allen, Acta Cryst. B 55 (1999) 1044.
[35] SPARTAN, SPARTAN'08, Wavefunction, Ver. 1.2.0., 18401 Von Karman Avenue, Suite Irvine, CA 92612, USA, 2009.
[36] A.D. Becke, Phys. Rev. A38 (1988) 3098.
[37] J.D. Perdew, Phys. Rev. B33 (1986) 8822.
[38] P.C. Hariharan, J.A. Pople, Theor. Chim Acta 28 (1973) 213.
[39] T.v. der Wijst, C.F. Guerra, M. Swart, F.M. Bickelhaupt, Chem. Phys. Lett. 426 (2006) 415.
[40] K.E. Riley, B.T.O. Holt, K.M. Merz Jr., J. Chem. Theory Comput. 3 (2) (2007) 407.
[41] A.D. Rabuck, G.E. Scuseria, Theor. Chim. Acta 104 (2000) 439.
[42] J.E. Del Bene, Encyclopedia of Computational Chemistry, vol. 1, Wiley, Chester, England, 1998. p. 1263.
[43] L. Hirsfeld, Theor. Chim. Acta 44 (1977) 129.
[44] S.K. Wolff, D.J. Grimwood, J.J. McKinnon, D. Jayatilaka, M.A. Spackman, CrystalExplorer, Version 2.1, University of Western Australia, Australia, 2007.
[45] E.W. Koneman, S.D. Allen, W.M. Janda, P.C. Screckenberger, W.C. Winn, Colour Atlas and Textbook of Diagnostic Microbiology, Lippincott-raven Publishers, Philadelphia, 1997.
[46] A.K. Bose, M.S. Manhas, M. Ghosh, V.S. Raju, K. Tabei, Z. Urbanczyklipkowska, Heterocycles 30 (1990) 741.
[47] T. Vidal, A. Petit, A. Loupy, R.N. Gedye, Tetrahedron 56 (2000) 5473.
[48] A. Stadler, B.H. Yousefi, D. Dallinger, P. Walla, E. Van der Eycken, N. Kaval, C.O. Kappe, Org. Process Res. Dev. 7 (2003) 707.
[49] H.D. Flack, Acta Cryst. A 39 (1983) 876.
[50] J. Bernstein, R.E. Davis, L. Shimoni, N.L. Chang, Angew. Chem. In. Ed. 34 (1995) 1555.
[51] G.R. Desiraju, T. Steiner, The Weak Hydrogen Bond in Structural Chemistry and Biology, Oxford University Press, Oxford, 1999.
[52] F.A. Cotton, L.M. Daniels, G.T. Jordan, C.A. Murillo, Chem. Commun. (1997) 1673.
[53] G.R. Desiraju, Encyclopedia of Supramolecular Chemistry, Marcel Dekker, New York, 2004.
[54] T. Steiner, Angew. Chem. In. Ed. 41 (2002) 48.
[55] T. Steiner, G.R. Desiraju, Chem. Commun. (1998) 891.
[56] J.J. Novoa, B. Tarron, M.H. Whangbo, J.M. Williams, J. Chem. Phys. 95 (1991) 5179.
[57] P. Seiler, L. Isaacs, F. Diederich, Helv. Chim. Acta 79 (1996) 1047.
[58] T. van Mourik, F.B. van Duijneveldt, Theochem. – J. Mol. Struct. 341 (1995) 63.
[59] X.J. Yan, S.M. Wang, M. Hodoscek, G.W.A. Milne, Theochem. – J. Mol. Struct. 115 (1994) 279.
[60] H. Bock, R. Dienelt, H. Schodel, Z. Havlas, J. Chem. Soc. – Chem. Commun. (1993) 1792.
[61] A. Cappelli, G. Giorgi, M. Anzini, S. Vomero, S. Ristori, C. Rossi, A. Donati, Chem. – Eur. J. 10 (2004) 3177.
[62] G.R. Desiraju, J. Chem. Soc. – Chem. Commun. (1990) 454.
[63] J.J. Novoa, F. Mota, Chem. Phys. Lett. 318 (2000) 345.
[64] S. Tsuzuki, K. Honda, T. Uchimaru, M. Mikami, K. Tanabe, J. Am. Chem. Soc. 122 (2000) 11450.
[65] W.L. Zhu, X.J. Tan, C.M. Puah, J.D. Gu, H.L. Jiang, K.X. Chen, C.E. Felder, I. Silman, J.L. Sussman, J. Phys. Chem. A104 (2000) 9573.
[66] C.J. Cramer, Essentials of Computational Chemistry Theories and Models, 2nd ed., Wiley, UK., 2004.
[67] C.C. Møller, M.S. Plesset, Phys. Rev. (1934) 618.
[68] J.J. McKinnon, D. Jayatilaka, M.A. Spackman, Chem. Commun. (2007) 3814.
[69] J.J. McKinnon, M.A. Spackman, A.S. Mitchell, Acta Cryst. B 60 (2004) 627.
[70] A.M. Pendas, V.L. Pueyo, E. Francisco, P.-M. Sanches, J. Chem. Phys. 3 (2002) 1017.
[71] E. Clementi, C. Roetti, At. Data Nucl. Data Tables 14 (1974) 177.